ARTICLE

All-Optical Wavelength Conversion by Picosecond Burst Absorption in Colloidal PbS Quantum Dots

Pieter Geiregat,[*,†,‡,§] Arjan J. Houtepen,[⊥,‡] Dries Van Thourhout,[†,§] and Zeger Hens[*,‡,§]

†Photonics Research Group, ‡Physics and Chemistry of Nanostructures, and §Center for Nano and Biophotonics, Ghent University, 9000 Ghent, Belgium

⊥Optoelectronic Materials Section, TU Delft, 2628 CD Delft, The Netherlands

Ⓢ Supporting Information

ABSTRACT: All-optical approaches to change the wavelength of a data signal are considered more energy- and cost-effective than current wavelength conversion schemes that rely on back and forth switching between the electrical and optical domains. However, the lack of cost-effective materials with sufficiently adequate optoelectronic properties hampers the development of this so-called all-optical wavelength conversion. Here, we show that the interplay between intraband and band gap absorption in colloidal quantum dots leads to a very strong and ultrafast modulation of the light absorption after photoexcitation in which slow components linked to exciton recombination are eliminated. This approach enables all-optical wavelength conversion at rates matching state-of-the-art convertors in speed, yet with cost-effective solution-processable materials. Moreover, the stronger light–matter interaction allows for implementation in small-footprint devices with low switching energies. Being a generic property, the demonstrated effect opens a pathway toward low-power integrated photonics based on colloidal quantum dots as the enabling material.

KEYWORDS: all-optical signal processing, nanocrystals, intraband absorption, transient absorption

All-optical signal processing is widely seen as a key enabler of high bit rate, low power, and cost-efficient data communication.[1,2] One of the basic functions involves the conversion of a data stream from a first (pump) to a second (probe) wavelength channel. This so-called wavelength conversion requires materials that show a strong and fast response of their optical constants at the probe wavelength to changes in light intensity at the pump wavelength. Published examples make use of phase modulation through χ_3 nonlinearities[3] or direct amplitude modulation.[4] Phase modulation effects are typically weak and require either long interaction lengths or complex interferometric configurations with the need for high input powers. Amplitude modulation makes use of epitaxially grown III–V semiconductors,[5] which are expensive and not directly compatible with a commercially interesting silicon-on-insulator platform.

To overcome these drawbacks, novel optoelectronic materials such as solution-processable colloidal quantum dots (QDs)[6,7] and graphene[8] have seen an increasing interest for applications in all-optical signal processing in general and wavelength conversion in particular. Li *et al.*[8] for example showed that carrier cooling in graphene leads to a picosecond,

broadband modulation of the absorption coefficient, yet the relatively weak interaction of graphene with light requires high input powers to achieve rather modest modulation depths of ≈0.3. Pacifici *et al.*[9] demonstrated a similar wavelength conversion scheme using the absorption of the probe light by intraband transitions in colloidal quantum dots (QDs) photoexcited by the pump light. Compared to graphene, QDs have larger absorption coefficients, possibly yielding a higher modulation depth and a smaller device footprint—yet the modulation rate will be limited by the single exciton recombination rate of ≈10^8 s^{-1} in II–VI QDs such as CdSe and CdTe[10] with a band gap in the visible range and ≈10^6 s^{-1} in IV–VI QDs such as PbS[11] and PbSe[12] with a band gap in the (near-)infrared range.

These limitations can be overcome by addressing multiexciton states, which show much faster recombination rates of ≈10^{11} s^{-1} due to Auger recombination.[13,14] Using the different stimulated emission rate of different multiexciton states, for

A

example, all optical modulation with a close to 1 THz 3 dB bandwidth was achieved using CdSe/ZnS QDs.[7] However, photoinduced changes linked to the formation of multiexciton states in QDs are highly nonlinear—and thus strongly power-dependent—and require high-power signals or, equivalently, a large energy per pulse. Moreover, the material response will still contain more slowly varying contributions due to the recombination of single excitons.

Here, we show that the trade-off between speed and nonlinearity when using colloidal QDs for all-optical signal processing is not inevitable. Using PbS QDs, we demonstrate that a specific probe wavelength range exists where the opposing effects of photobleaching, photoinduced absorption,[15] and spectral shifts[16] in photoexcited QDs cancel, apart from the first picosecond following photoexcitation by the pump pulse. We show that this results in an intense, linear, and ultrafast burst of photoinduced absorption that maintains its characteristics under excitation using 450 and 225 Gb/s pulse trains. We argue that this makes colloidal QDs an ideal material for low-power, picosecond wavelength conversion that can be used in small-footprint, integrated photonic devices.

RESULTS

Light Absorption by Photoexcited PbS Quantum Dots. We make use of 4.6 nm PbS QDs synthesized according to established literature procedures.[17,18] The dots are diluted in hexane for all measurements, unless mentioned otherwise. Their absorption spectrum (see Figure 1a, solid black line)
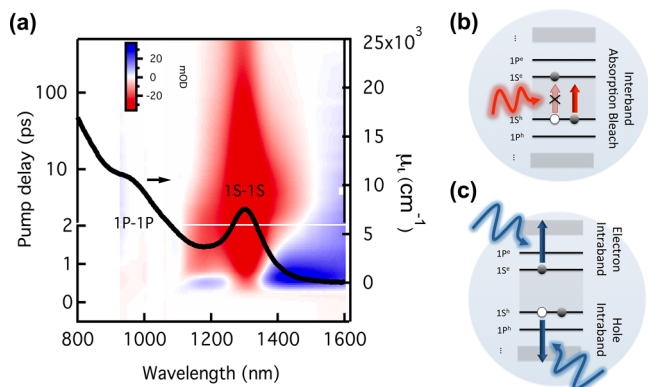
Figure 1. Overview. (a) Two-dimensional time-wavelength map of band-edge differential absorbance spectrum ΔA after 700 nm photoexcitation, creating on average 0.93 excitons per QD. Also, the intrinsic absorption spectrum μ_i of 4.6 nm PbS QDs dispersed in hexane is shown (solid black line). The lowest-energy exciton transitions are labeled 1P-1P and 1S-1S. (b,c) Schematic depicting the two relevant ultrafast processes discussed in this work: interband bleach (b) and intraband absorption (c) for a nanocrystal with a single 1S-1S exciton (here two-fold degenerate for simplicity).

features the typical characteristic of optical transitions between size-quantized levels in the valence and the conduction band, labeled as 1S-1S and 1P-1P. In addition, Figure 1a shows the differential absorbance ΔA for the same QDs following a 180 fs, 700 nm pump pulse that creates on average 0.93 excitons per QD (denoted further as $\langle N \rangle = 0.93$; see Methods) as a time-wavelength intensity map around the 1S-1S band-edge transitions. Focusing first on the differential absorbance at delay times longer than ≈ 1 ps, one notices a strong reduction

of the absorption (bleach, negative differential absorbance, Figure 1b) at around 1300 nm, which reflects the occupation of the band-edge states (state filling) by electrons and holes. The decay of the band gap bleach observed between 1 and 100 ps is well described by a single-exponential function with a time constant of 43 ps and is typically attributed to Auger recombination of multiexcitons.[19,20] At wavelengths longer than 1500 nm on the other hand, a relatively weak photoinduced absorption is observed. This shows the same decay dynamics as the band gap bleach and has been attributed before to intraband transitions involving the cooled electron and hole that occupy the band-edge states (see Figure 1c).[15]

A markedly different differential absorbance spectrum appears within the first picosecond after photoexcitation. Here, the photoinduced absorption is considerably stronger and extends over a much wider range of wavelengths. This initial dynamics has been attributed to exciton cooling by De Geyter et al., where it was concluded that a hot exciton shows considerably stronger intraband absorption than a cold exciton.[15] In addition, the decrease of the biexciton addition energy upon exciton cooling and the concomitantly reduced red shift of the absorption spectrum[16,21] will contribute to the change of the photoinduced absorption close to the band gap transition. A more detailed analysis, however, shows that the main contribution to the photoinduced absorption at longer wavelengths must be due to intraband absorption since the linear absorption is nearly zero at those wavelengths.

Matching State Filling and Intraband Transitions. The interplay between hot carrier intraband absorption and band gap bleach during exciton cooling can be analyzed in more detail using spectral cuts of the transient absorbance taken at fixed delay times, as represented in Figure 2a. At early times (0.3–0.6 ps), photoinduced absorption ($\Delta A > 0$) by hot excitons is pronounced and the band gap bleach is limited since exciton cooling is far from complete. As a result, the differential absorbance is strong and positive apart from a small region around the band gap transition. After exciton cooling (2–2.5 ps), the photoinduced absorption is reduced and the band gap bleach ($\Delta A < 0$) has become more distinct. As a result, a net photoinduced absorption is only attained at wavelengths well beyond the band gap transition. In a later stage (2.5–100 ps), multiexciton recombination further reduces the differential absorbance without, however, inducing significant spectral changes.

A remarkable point made clear by the spectral cuts shown in Figure 2a concerns the wavelength at which the opposing effects of photoinduced absorption by intraband transitions and photobleaching by state filling yield a zero net differential absorption. Since both change during exciton cooling, this matching wavelength λ_m obviously shifts during the first 1–2 ps after photoexcitation. More importantly, however, is that this matching wavelength stays constant at $\lambda_m = 1520$ nm for longer pump–probe delay times, without being affected by multi-exciton recombination. Knowing the origin of the opposing effects—the presence of excitons opening up intraband transitions and blocking interband transitions—this can be readily explained. Indeed, as all effects scale proportionally to the average exciton number $\langle N \rangle$, λ_m should be independent of $\langle N \rangle$.

The significance of the matching wavelength being independent of $\langle N \rangle$ can be appreciated better by looking at vertical cuts of Figure 1a, taken at different wavelengths (see Figure 2b). At wavelengths shorter than λ_m, the initially strong
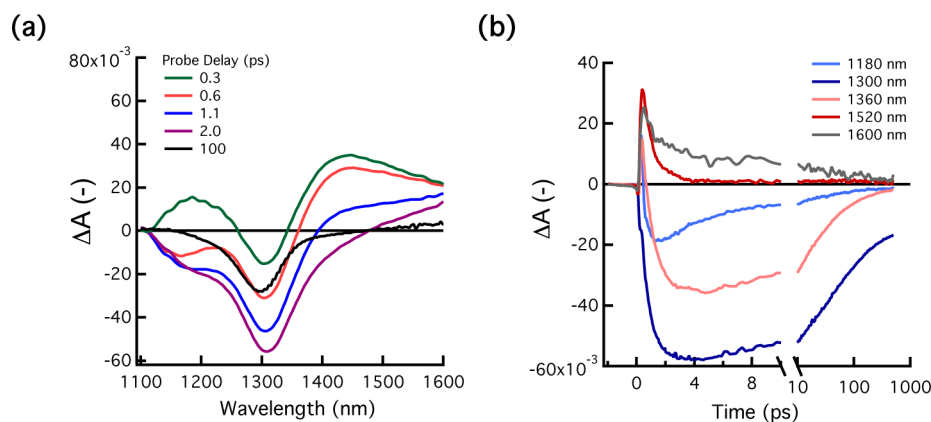
Figure 2. Kinetics and spectra of differential absorbance ΔA. (a) Spectra at different probe delays obtained from horizontal cuts of Figure 1b and (b) kinetic traces at different wavelengths (vertical cuts of Figure 1b).
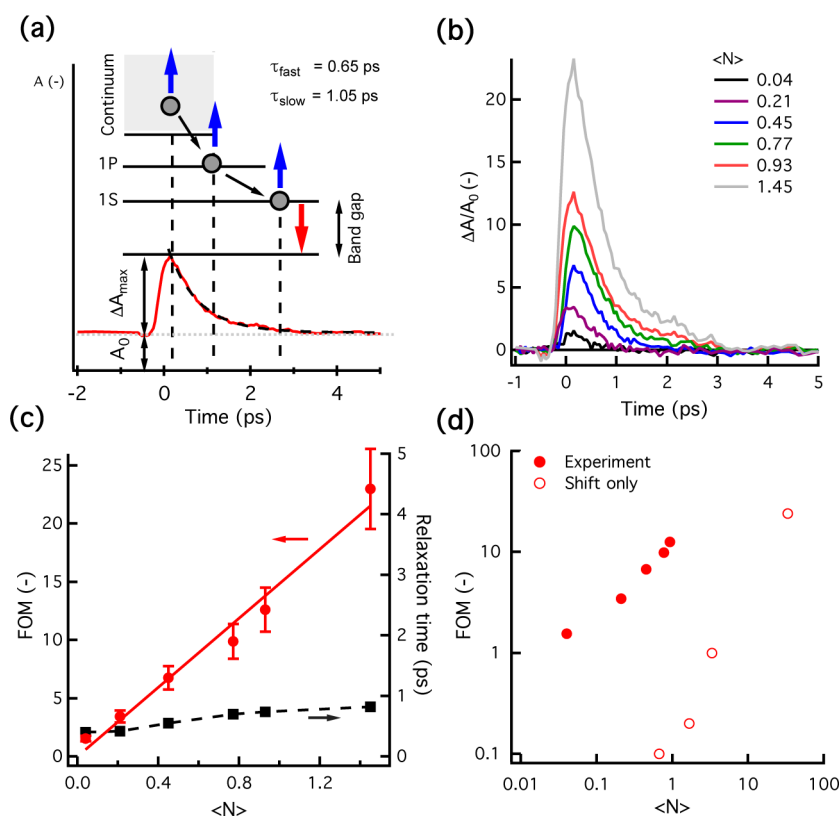

Figure 3. Pump power dependence. (a) Schematic of proposed mechanism of 1P-1S limited hot carrier cooling in relation the observed response at the matching wavelength. A biexponential fit yields a fast and slow relaxation rate of 0.65 and 1.05 ps, respectively. (b) Transients of differential absorbance ΔA normalized to the linear absorbance A_0 for increasing pump fluence as expressed by increasing average exciton population $\langle N \rangle$. (c) FOM (red circles), the maximum of the $\Delta A/A_0$ transients of panel (b), for increasing fluence plotted with decay constant (black squares). A linear fit (FOM = $C \times \langle N \rangle$) to the data is shown (solid red line). (d) Expected FOM for a case of pure spectral shifting, calculated according to Geiregat et al.[16] A shift of 3 meV was used per created exciton. We clearly see that the observed modulation is much stronger (up to 2 orders of magnitude) than ever to be expected from multi-X-induced shifts. This confirms the idea of competition of interband bleach with (hot and cold carrier) intraband absorption only.

and positive transient absorption quickly decays with the cooling rate to reach a negative value, the subsequent time evolution of which reflects the decay of multiexcitons and, eventually, single excitons. Opposite from this, a residual photoinduced absorption remains after exciton cooling at wavelengths longer than λ_m on which the exciton recombination dynamics is imprinted, as well. However, at the matching wavelength, the initial differential absorption drops to zero within 1−2 ps to remain zero, irrespective of further exciton

recombination. At this wavelength, ensembles of unexcited and excited QDs containing cold band-edge excitons have the same absorption coefficient, and therefore, further exciton recombination has no effect on the absorption coefficient.

Intense, High Figure-of-Merit Absorption Bursts. Figure 3a presents a closer look at the time-dependent absorption $A(t) = A_0 + \Delta A(t)$ at the matching wavelength, following a $\langle N \rangle = 0.93$ excitation at 700 nm. Transients at different pump wavelengths are shown in the Supporting

C
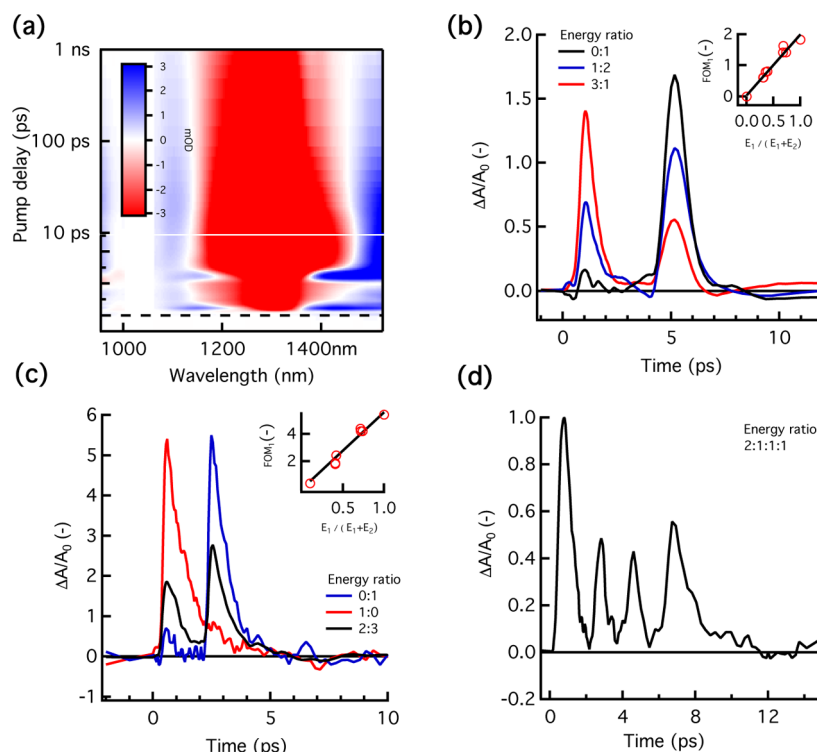
Figure 4. Ultrashort refresh times. (a) Two-dimensional time-wavelength map of pump−repump−probe experiment with 4.4 ps separation between pump and repump. (b,c) Kinetics at matching wavelength for different input combinations (expressed as the energy distribution between both pump pulses; *e.g.*, 1−1 indicates equal energies in both pulses, *etc.*), showing the ability of the system to refresh after 4.4 ps (b) and 2.2 ps (c). Insets of (b,c) show the relation between $\Delta A_{max}/A_0$ of the first pulse *versus* the relative energy in the first pulse together with a linear fit through zero, indicating a linear response of the system. (d) Four-pulse experiment showing the ability to process multiple pulses at a rate of *ca.* 450 Gb/s.

Information (Figure S2). Following photoexcitation, the absorption increases rapidly to reach a maximum value $A_0 + \Delta A_{max}$, after which it returns back to A_0 by a decay that can be fitted to a double-exponential with time constants of 0.65 and 1.05 ps. As shown in Figure 3a, this two-component decay may reflect the successive cooling of the hot carriers from the higher energy continuum of electron or hole states to the size-quantized P states, followed by further cooling to the band-edge S states by, among other proposed mechanisms, phonon- or Auger-assisted relaxation.[22]

In Figure 3a, the transient absorption ΔA at the matching wavelength as recorded for different pump fluences is plotted normalized relative to the absorbance A_0 at λ_m. The ratio $\Delta A/A_0$ reflects the light intensity of a probe signal at λ_m that is additionally absorbed after excitation of the QDs by a pump pulse (although in all cases absorption at λ_m is meant, any reference to the matching wavelength is omitted for clarity):

$$\frac{\Delta A}{A_0} = \frac{\log(I_{t,0}) - \log(I_{t,p})}{\log(I_0) - \log(I_{t,0})} \qquad (1)$$

Here, I_0 is the incident light intensity while $I_{t,0}$ and $I_{t,p}$ are the transmitted intensity in the absence and presence of the pump pulse, respectively. Figure 3c shows that the ratio $\Delta A_{max}/A_0$—a number we will use as a figure-of-merit (FOM) since it is independent of sample geometry—scales proportionally to $\langle N \rangle$ (red circles, Figure 3c) and reaches a value as high as 23 for $\langle N \rangle$ = 1.3 without any sign of saturation. Moreover, the ultrafast decay rate (black squares, Figure 3c) is largely independent of $\langle N \rangle$ at ≈1 ps. We thus conclude that the $\Delta A/A_0$ transient is a linear function of the pump intensity that provides an ultrafast

and intense increase of the extinction of a probe beam at the matching wavelength in the presence of a pump beam. Note that nothing limits the FOM as defined here from exceeding unity at λ_m since it compares photoinduced absorption to the residual band gap absorption at that wavelength. These are different processes to which either all photoexcited QDs contribute or only a small fraction of relatively large QDs.

As mentioned before, spectral shifts could also contribute to the observed photoinduced absorption. However, spectral shifts only influence those spectral regions with strong gradients in the linear absorption.[16] Using the formula (see Supporting Information S1) put forward by Geiregat *et al.*,[16] we can estimate the FOM that would be achieved by a pure shift-induced photoinduced absorption. Figure 3d shows this FOM (empty circles) for a shift of 3 meV (other values are presented in the Supporting Information S1) per created exciton, a reasonable number for cold excitons, together with the experimental FOM for varying pump fluence, expressed as $\langle N \rangle$. The plot clearly shows that the observed FOM is more than 1 order of magnitude larger than predicted by the shift-only model. This confirms the conclusion already made that the observed matching effect mainly involves a balancing of bleach and intraband absorption with only a negligibly small contribution from spectral shifts.

Ultrashort Refresh Times. If the $\Delta A/A_0$ transient can indeed be seen as the response of a linear system following a pulsed excitation, a series of successive light pulses separated by a time delay longer than the transient decay should lead to a sequence of absorption bursts at λ_m. With a decay time of 1.3 ps, this would correspond to pulse frequencies close to 1 THz.
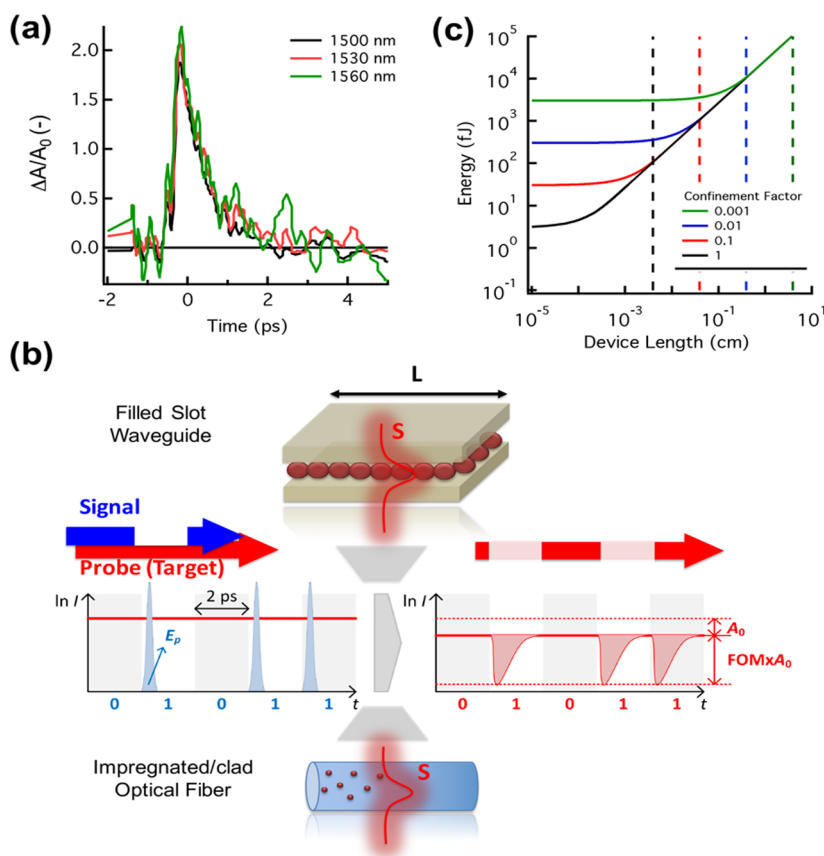
Figure 5. Integration with photonic devices. (a) Demonstration of burst absorption in thin (75 nm) spin-coated film of QDs on a glass substrate $\langle N \rangle$. (b) Wavelength conversion scheme with incident pump (or signal, dashed blue)/probe (or target, solid red) sequence and corresponding output indicating the meaning of the FOM, using either a typical integrated SOI design with slot waveguide ($\Gamma = 0.1$) containing nanocrystals or a impregnated or QD-covered glass fiber ($\Gamma = 0.001$). (c) Evaluation of switching energy per bit (in femtojoule) and device interaction length (in cm) for a variety of optical confinement factors with 3 dB exctinction (vertical dashed lines) of the target wave without pump pulse present. Additional calculations are available in the Supporting Information.

To investigate this, we have pumped the samples with trains of 2 or 4 pulses—created by passing the pump pulse through a polarizer and a birefringent crystal (see Methods and Supporting Information S4)—in which each pulse is separated by only 2.2 or 4.4 ps, delays we hitherto denote as short and long.

The transient absorption map for a long delay, two-pulse excitation is represented in Figure 4a. It can be clearly seen that the second pump pulse at 4.4 ps again induces a strong, broadband photoinduced absorption at λ_m due to intraband transitions linked to the newly created hot excitons. As a result, the $\Delta A / A_0$ transients shown in Figure 4b are composed of a sequence of two clearly distinguishable absorption bursts separated by 4.4 ps. By varying the polarization angle of the pump light (see Supporting Information S4), the distribution of the initial pump intensity over both pulses can be varied, mimicking, for example, bit patterns such as 1−0 and 0−1. As demonstrated by Figure 4b, this leads to a proportional variation of $\Delta A / A_0$ induced by either of the pulses (see also insets of Figure 4b,c). This is clear proof that the linearity between peak absorbance and pump power is indeed maintained for a two-pulse excitation. Importantly, the same conclusion applies when reducing the time separation between two successive pulses to 2.2 ps (see Figure 4c), with a similar linear dependence of $\Delta A / A_0$ on either of the pulse intensities. Moreover, as shown by Figure 4d, also a four-pulse excitation

with 2.2 ps delay is converted into four absorption bursts at the matching wavelength.

Small-Footprint, Low-Energy per Pulse Wavelength Conversion. Since ΔA scales proportionally to $\langle N \rangle$, a transient intrinsic absorption coefficient $\Delta \mu_i$, which is the transient absorption coefficient of a fictitious material in which QDs containing a single exciton are packed with a volume fraction $f = 1$, can be defined at the matching wavelength as (see Methods)[23]

$$\Delta \mu_i = \frac{\text{FOM}}{\langle N \rangle} \mu_i \approx 14 \times \mu_i \tag{2}$$

Knowing the intrinsic absorption coefficient μ_i of PbS QDs at λ_m (see Figure 1a, solid black curve, $\mu_{i,\lambda_m} = 371$ cm^{-1}), we find that $\Delta \mu_i$ attains a maximum of 5200 cm^{-1}. Assuming a QD volume fraction f of 0.2—a typical value for a QD thin film— this implies that a pump pulse creating an exciton density of $\langle N \rangle = 1$ only needs a 10 μm thick QD film to achieve a $1/e$ attenuation of the probe beam with a FOM of 14 at a time scale of 1 ps. Importantly, as confirmed by Figure 5a for a fluence of $\langle N \rangle = 0.1$, such QD films indeed show a burst absorption at the matching wavelength similar to dilute QD dispersions, both in terms of speed and FOM.

The combination of this considerable absorption burst, the fast absorption decay, and ultrafast refresh times could make QDs ideally suited to convert a high bit rate optical signal

carried by the pump beam to a probe beam at λ_m over micrometer distances. A possible implementation of this so-called all-optical wavelength conversion is sketched in Figure 5b. Here, a light pulse in the pump beam induces a burst of absorption of probe light in the QD film, thus transferring a sequence of intensity pulses into intensity dips. Given the characteristics of the ΔA transient, this conversion scheme could operate at bit rates approaching 1 THz. Moreover, the ultrafast return of the absorption transient to A_0 makes this conversion happen without spurious residual absorption, which would induce detrimental patterning effects typically seen in modulators without such return-to-zero. The importance of this can be readily seen from the transient absorption at wavelengths longer than λ_m, where the uncompensated background of photoinduced absorption after the pump pulse accumulates pulse after pulse (see Supporting Information, Figure S6). This reduces the ΔA contrast, and therefore, a single pulse cannot be linked to a unique absorption change.

The possibility of wavelength conversion of compact optical modes over short interaction lengths by QD films can be exploited most advantageously in silicon or silicon-nitride-based integrated waveguide platforms.[3,24,25] These have become increasingly popular since the high-index contrast enables very compact devices to be fabricated by mature CMOS processing techniques. In addition, they offer the possibility for monolithic electronic–photonic interfaces, which could lead to important savings in cost and power consumption. However, the refractive index of silicon and silicon nitride exhibits only weak dependence on the light intensity precluding the realization of efficient all-optical switches and wavelength convertors.

To assess the potential of such an integrated wavelength convertor, we modeled its FOM while characterizing the convertor by a mode area S, a modal confinement factor Γ— denoting the fraction of the power confined in the QD layer—a waveguide length L and the energy per bit E_p of the carrier, that is, per pump pulse. We note that the contribution of spontaneous emission to the FOM can be neglected due to the long radiative lifetime of the QDs; see Supporting Information (S8). The main characteristics are shown in Figure 5c, where the energy per bit required for reaching a FOM of 5 is plotted as a function of the interaction length for a fixed active area and different confinement factors. More detailed calculations, in line with the possible implementation of the convertor as a PbS QD film sandwiched between two Si waveguides or a QD-coated optical fiber, are shown in the Supporting Information (S6). The dashed vertical lines in Figure 5c indicate carrier losses of 3 dB in the absence of the pump pulse for the different confinement factors (0.001–0.1), which is a reasonable operation point. The calculations confirm that wavelength conversion over interaction lengths as short as 10–100 μm should be possible with energies as low as 10–100 fJ per pulse when using small area optical modes with high confinement factors. This figure matches the state-of-the-art[26] yet with substantially shorter interaction lengths. Reducing the confinement factor increases the interaction length and also raises the required energy per pulse to keep the wavelength conversion characteristics constant.

The short interaction lengths and low energy per pulse required for integrated conversion makes the burst absorption of colloidal QDs very relevant for novel integrated devices based on colloidal QDs, potentially outperforming other materials such as graphene,[8] III–V epitaxial semiconductors,[5]

and small-molecule organics[26] in terms of speed, energy per bit, and device footprint. Moreover, the approach developed has considerable advantages as compared to recently suggested alternative schemes to perform ultrafast all-optical wavelength conversion or (more general) signal manipulation using QDs. Saari et al.,[7] for example, used a three-beam approach to modulate visible (560–600 nm) light pulses using CdSe/ZnS QDs. Apart from a pump and a probe, they used a saturator to fully occupy the first exciton transition, requiring at least two electron–hole pairs per dot on average. This increases not only the complexity of the conversion scheme but also its power consumption. Moreover, relying on multiexcitons increases nonlinearity between input and output and results in spurious residual signals due to the different time scales of their recombination. Gao et al.,[14] on the other hand, proposed to use coupled films of PbSe QDs. In these films, carrier accumulation in the largest dots of an ensemble depletes the smaller QDs on a picosecond time scale. This approach, however, only works after specific ligand processing, increasing complexity of fabrication. Moreover, the observed effect will be weak, making the scheme ill-suited for small-footprint devices, as only a few QDs in the entire film are active.

CONCLUSION

We have demonstrated that the interplay of intrinsic QD properties such as interband bleach and intraband absorption leads to ultra-low-power picosecond all-optical wavelength conversion using colloidal PbS QDs. It sheds a positive light on intraband absorption as a very useful feature when designing colloidal QD-enhanced photonic components. The mechanism is ultrafast (ca. 1 ps) and linear in the pump power. Moreover, it occurs for overall exciton densities far below unity and leaves no residual background, a long-standing issue in QD-based wavelength convertors. In addition, the effect was demonstrated in the near-infrared, a part of the spectrum relevant for optical datacommunication. Multipulse sequences (up to 450 Gb/s) were used to study the behavior under pulse-train excitation, a situation relevant for actual all-optical wavelength conversion in a high bit rate context. With this work, we have shown the possibility to enhance the ultrafast and nonlinear dynamics of existing photonic platforms (such as silicon-on-insulator) with QDs, a relatively unexplored approach so far. Future work in this direction should aim for an on-chip demonstrator of the ideas and concepts validated in this work.

METHODS

Materials. Oleylamine (OLA)-capped PbS QDs were synthesized using the procedure described by Cademartiri et al.[18] and modified by Moreels et al.[27] After synthesis, the OLA ligand shell is substituted by oleic acid (OA). An exchange to OA is typically performed by adding OA to a toluene suspension of PbS QDs in a ratio of 1.5:10 OA/toluene. After precipitation with ethanol and centrifugation, the QDs are resuspended in toluene and the exchange is repeated. Thin films are fabricated using spin-coating from a dilute solution at 2000 rpm on silica glass substrates. Film thickness is obtained from atomic force microscopy analysis and optical measurements.

White Light Pump–Probe Spectroscopy. Samples were pumped using 180 fs pulses at 700–1100 nm, created from the 1028 nm fundamental (Pharos SP, 6 W, Light Conversion) through nonlinear frequency mixing in an OPA (Orpheus, Light Conversion). Probe pulses were generated in a sapphire crystal using the 1028 nm fundamental. The pulses were delayed relative to the probe using a delay stage with maximum delay of 2.5 ns (Helios Spectrometer, Ultrafast Systems). The probe spectrum covers the vis–NIR window

from 450 to 1620 nm. PbS nanocrystals were dispersed in a transparent solvent (hexane) to achieve optical densities of *ca.* 0.1 at the first exciton transition. Samples were not stirred during the measurements. No difference was observed with stirring, indicating an absence of photocharging under the used pump fluences. Assuming a Poisson distribution of the carrier population after photoexcitation, the probability P_N to have N excitations in one nanocrystal is given by

$$P_N = \frac{e^{-\langle N \rangle} \langle N \rangle^N}{N!} \tag{3}$$

where $\langle N \rangle$ is the mean exciton number determined as $\langle N \rangle = J_{ph} \times \sigma_p$, with J_{ph} the photon flux (photons/cm^2) and the cross section σ_p at the pump wavelength, determined starting from $\mu_{i,400}$ as[23]

$$\sigma_p = V_{QD} \times \mu_{i,400} \times \frac{A_{0,p}}{A_{0,400}} \times \frac{1 - 10^{-A_{0,p}}}{10^{-A_{0,p}}} \tag{4}$$

where V_{QD} is the QD volume and $A_{0,i}$ (i = p,400) is the linear absorbance at the pump (p) wavelength and 400 nm. The last factor corrects for pump beam attenuation when propagating through the cuvette.

Pulse Sequence Generation. The initial 180 fs pulse is linearly polarized under a desired angle using a half-wave plate and sent through a combination of birefringent YVO$_4$ crystals to create a cascade of two pulses separated by the group delay imposed through the difference in refractive index between ordinary and extraordinary waves.[28] The pulses are then sent through a depolarizer to avoid any polarization-induced effects. By varying the polarization angle, we can divide the initial pulse energy over both pulses on demand as is explained in the Supporting Information, section S3 (*i.e.*, continuously from 1 to 0 to 0−1). No substantial pulse broadening is observed after propagation through the crystal sequence. To create four pulses, an additional rotation through a second half-wave plate is used in combination with a third birefringent crystal. This allows us to create four pulses separated by 2.2 ps without the need for additional delay stages or optics.

ASSOCIATED CONTENT

ⓢ Supporting Information

The Supporting Information is available free of charge on the ACS Publications website at DOI: 10.1021/acsnano.5b06630.

> General description of the analysis of spectral shifts, synthesis protocols, information on multipulse generation, varying pump wavelength experiments, discussion of the intrinsic absorption coefficient, and a detailed calculation of the switching energy (PDF)

AUTHOR INFORMATION

Corresponding Authors
*E-mail: Pieter.Geiregat@UGent.be.
*E-mail: Zeger.Hens@UGent.be.

Notes
The authors declare no competing financial interest.

REFERENCES

(1) Alduino, A.; Paniccia, M. Wiring Electronics with Light. *Nat. Photonics* 2007, 1, 153−155.

(2) Yoo, S. Wavelength Conversion Technologies for WDM Network Applications. *J. Lightwave Technol.* 1996, 14, 955−966.

(3) Leuthold, J.; Koos, C.; Freude, W. Nonlinear Silicon Photonics. *Nat. Photonics* 2010, 4, 535−544.

(4) Durhuus, T.; Mikkelsen, B.; Joergensen, C. All-Optical Wavelength Conversion by Semiconductor Optical Amplifiers. *J. Lightwave Technol.* 1996, 14, 942−954.

(5) Leuthold, J.; Moller, L.; Jaques, J. 160 Gbit/s All-Optical Wavelength Converter and Assessment of Its Regenerative Properties. *Electron. Lett.* 2004, 40, 554−555.

(6) Talapin, D. V.; Lee, J.-S.; Kovalenko, M. V.; Shevchenko, E. V. Prospects of Colloidal Nanocrystals for Electronic and Optoelectronic Applications. *Chem. Rev.* 2010, 110, 389−458.

(7) Saari, J. I.; Krause, M. M.; Walsh, B. R.; Kambhampati, P. Terahertz Bandwidth All-Optical Modulation and Logic Using Multiexcitons in Semiconductor Nanocrystals. *Nano Lett.* 2013, 13, 722.

(8) Li, W.; Chen, B.; Meng, C.; Fang, W.; Xiao, Y.; Li, X.; Hu, Z.; Xu, Y.; Tong, L.; Wang, H.; Liu, W.; Bao, J.; Shen, Y. R. Ultrafast All-Optical Graphene Modulator. *Nano Lett.* 2014, 14, 955−959.

(9) Pacifici, D.; Lezec, H. J.; Atwater, H. a. All-Optical Modulation by Plasmonic Excitation of CdSe Quantum Dots. *Nat. Photonics* 2007, 1, 402−406.

(10) Gong, K.; Zeng, Y.; Kelley, D. F. Extinction Coefficients, Oscillator Strengths, and Radiative Lifetimes of CdSe, CdTe, and CdTe/CdSe Nanocrystals. *J. Phys. Chem. C* 2013, 117, 20268−20279.

(11) Justo, Y.; Geiregat, P.; Hoecke, K. V.; Vanhaecke, F.; De Mello Donega, C.; Hens, Z. Optical Properties of PbS/CdS Core/Shell Quantum Dots. *J. Phys. Chem. C* 2013, 117, 20171−20177.

(12) De Geyter, B.; Justo, Y.; Moreels, I.; Lambert, K.; Smet, P. F.; Van Thourhout, D.; Houtepen, A. J.; Grodzinska, D.; de Mello Donega, C.; Meijerink, A.; Vanmaekelbergh, D.; Hens, Z. The Different Nature of Band Edge Absorption and Emission in Colloidal PbSe/CdSe Core/Shell Quantum Dots. *ACS Nano* 2011, 5, 58−66.

(13) Klimov, V. I. Quantization of Multiparticle Auger Rates in Semiconductor Quantum Dots. *Science* 2000, 287, 1011−1013.

(14) Gao, Y.; Sandeep, C. S. S.; Schins, J. M.; Houtepen, A. J.; Siebbeles, L. D. a. Disorder Strongly Enhances Auger Recombination in Conductive Quantum-Dot Solids. *Nat. Commun.* 2013, 4, 2329.

(15) De Geyter, B.; Houtepen, A. J.; Carrillo, S.; Geiregat, P.; Gao, Y.; Ten Cate, S.; Schins, J. M.; Van Thourhout, D.; Delerue, C.; Siebbeles, L. D.; Hens, Z. Broadband and Picosecond Intraband Absorption in Lead-Based Colloidal Quantum Dots. *ACS Nano* 2012, 6, 6067−6074.

(16) Geiregat, P.; Houtepen, A.; Justo, Y.; Grozema, F. C.; Van Thourhout, D.; Hens, Z. Coulomb Shifts upon Exciton Addition to Photoexcited PbS Colloidal Quantum Dots. *J. Phys. Chem. C* 2014, 118, 22284−22290.

(17) Moreels, I.; Justo, Y.; De Geyter, B.; Haustraete, K.; Martins, J. C.; Hens, Z. Size-tunable, Bright, and Stable PbS Quantum Dots: A Surface Chemistry Study. *ACS Nano* 2011, 5, 2004−2012.

(18) Cademartiri, L.; Montanari, E.; Calestani, G.; Migliori, A.; Guagliardi, A.; Ozin, G. a. Size-Dependent Extinction Coefficients of PbS Quantum Dots. *J. Am. Chem. Soc.* 2006, 128, 10337−46.

(19) Schaller, R. D.; Petruska, M. a.; Klimov, V. I. Tunable Near-Infrared Optical Gain and Amplified Spontaneous Emission Using PbSe Nanocrystals. *J. Phys. Chem. B* 2003, 107, 13765−13768.

(20) Stewart, J. T.; Padilha, L. a.; Qazilbash, M. M.; Pietryga, J. M.; Midgett, A. G.; Luther, J. M.; Beard, M. C.; Nozik, A. J.; Klimov, V. I. Comparison of Carrier Multiplication Yields in PbS and PbSe Nanocrystals: the Role of Competing Energy-loss Processes. *Nano Lett.* 2012, 12, 622−8.

(21) Klimov, V.; Hunsche, S.; Kurz, H. Biexciton Effects in Femtosecond Nonlinear Transmission of Semiconductor Quantum Dots. *Phys. Rev. B: Condens. Matter Mater. Phys.* 1994, 50, 8110.

(22) Pandey, A.; Guyot-Sionnest, P. Slow Electron Cooling in Colloidal Quantum Dots. *Science* 2008, 322, 929−32.

(23) Hens, Z.; Moreels, I. Light Absorption by Colloidal Semiconductor Quantum Dots. *J. Mater. Chem.* 2012, 22, 10406−10415.

(24) Rickman, A. The Commercialization of Silicon Photonics. *Nat. Photonics* 2014, 8, 579−582.

(25) Simply Silicon. *Nat. Photonics* **2010**, *4*, 491; DOI: 10.1038/nphoton.2010.190

(26) Koos, C.; Vorreau, P.; Vallaitis, T.; Dumon, P.; Bogaerts, W.; Baets, R.; Esembeson, B.; Biaggio, I.; Michinobu, T.; Diederich, F.; Freude, W.; Leuthold, J. All-Optical High-Speed Signal Processing with Silicon-Organic Hybrid Slot Waveguides. *Nat. Photonics* **2009**, *3*, 216−219.

(27) Moreels, I.; Lambert, K.; Smeets, D.; De Muynck, D.; Nollet, T.; Martins, J. C.; Vanhaecke, F.; Vantomme, A.; Delerue, C.; Allan, G.; Hens, Z. Size-dependent Optical Properties of Colloidal PbS Quantum Dots. *ACS Nano* **2009**, *3*, 3023−30.

(28) Zhou, S.; Ouzounov, D.; Li, H.; Bazarov, I.; Dunham, B.; Sinclair, C.; Wise, F. W. Efficient Temporal Shaping of Ultrashort Pulses with Birefringent Crystals. *Appl. Opt.* **2007**, *46*, 8488−92.